CHEMISTRY OF MATERIALS
Article
pubs.acs.org/cm

Synthesis of Monodisperse Polystyrene@Vinyl-SiO_2 Core−Shell Particles and Hollow SiO_2 Spheres

Tian-Song Deng and Frank Marlow*

Max-Planck-Institut für Kohlenforschung, Kaiser-Wilhelm-Platz 1, 45470 Mülheim an der Ruhr, Germany

Supporting Information

ABSTRACT: This paper presents a scalable method of preparing highly monodisperse core−shell particles and hollow spheres, and their application in fabricating colloidal crystals. By using polystyrene (PS) particles as the template and vinyltrimethoxysilane as the precursor, the core−shell particles could be obtained via direct growth of vinyl-SiO_2 hybrid material on the negatively charged PS template. This method has two interesting characteristics. The first is the tunable shell thickness (from 10 to 170 nm) combined with a low polydispersity (smaller than 3%). Second, the method is simpler than traditional ones, which use surface modified PS as template to get a uniform coating. Furthermore, the core−shell particles could be converted into hollow SiO_2 spheres by removing the PS cores in a calcination process. Both the PS@vinyl-SiO_2 particles and the hollow SiO_2 spheres could be self-assembled into three-dimensional colloidal crystals, because the resulting particles are highly monodisperse and suspensible.

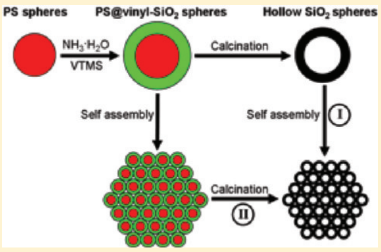

KEYWORDS: *core−shell, hollow SiO_2 spheres, colloidal crystals, monodisperse*

1. INTRODUCTION

SiO_2-coated particles have been attracted much attention, because these core−shell particles have potential applications in catalysis, drug delivery, and colloidal crystals.[1−5] As a coating material, SiO_2 has many versatile properties. First of all, SiO_2 is hydrophilic and negatively charged, which can prevent the aggregation of the colloidal particles. Hollow silica structures could be obtained by removing the core material via calcination or leaching, because the SiO_2 is chemically very stable. Furthermore, SiO_2 has also a tunable controlled porosity, biocompatibility, optical transparency, and mechanical stability.[1,2] Thus, SiO_2 is considered as an ideal and low-cost material that has already been used for coating on various core particles, such as metal colloids (e.g., Au, Ag),[6,7] magnetic particles (e.g., Fe_3O_4),[8] semiconductor nanocrystals (e.g., CdTe),[9] and polymers (e.g., polystyrene).[10−19]

Among these core particles, polymers such as polystyrene (PS) are a widely used particles that have uniform spherical shape, high monodispersity, and a large particle size range.[1,2] The Stöber method[20] can be used for SiO_2 coating on the surface of PS particles, if one handles the surface charge appropriately. For example, Xia et al.[10] used a positively charged PS and coated a uniform silica shell on their surface. Normally, both the SiO_2 particles[1,2] and many commonly used PS particles are negatively charged.[15] Direct coating of SiO_2 on negatively charged PS particles resulted in SiO_2 nanoparticles randomly distributed on the PS surface as well as in many free SiO_2 particles in the product.[10] To get smooth and homogeneous core−shell structures, the negatively charged surface of PS particles has to be modified.[11−16]

Blaaderen et al.[13] demonstrated a general method to coat colloids with SiO_2 by adsorbing poly(vinylpyrrolidone) (PVP) on the surface of colloidal particles. Chiu et al.[15] demonstrated the coating of SiO_2 on a polyelectrolyte (positively charged) deposited PS particles (negatively charged). Bourgeat-Lami et al.[16] reported SiO_2 coating on SiOH-functionalized PS, by using 3-(trimethoxysilyl)-propyl methacrylate as a functional comonomer during PS latex synthesis. In all of these reports, uniform SiO_2 shells were coated on positively charged surfaces, PVP-stabilized surfaces, or SiOH-functionalized surfaces but not on native, negatively charged surfaces. However, some of these approaches involving surface modifications do not work so perfectly. For example, in ref 10, the particles have an enhanced roughness and the fabricated colloidal crystal has a low quality.

A versatile method of preparing highly monodisperse organo silica hybrid spheres,[21] and their application in colloidal crystals,[22,23] has been reported. It uses vinyltrimethoxysilane as a precursor in presence of ammonia catalyst. Now, we extend this synthetic method to the direct coating of a uniform vinyl-functionalized SiO_2 shell on negatively charged PS particles (PS@vinyl-SiO_2). Highly monodisperse PS@vinyl-SiO_2 core−shell particles and hollow SiO_2 spheres were prepared and assembled into colloidal crystals (Scheme 1). The thickness of the vinyl-SiO_2 shell could be adjusted from 10 to 170 nm by the concentration of precursor. The polydispersity of the core−shell particles was smaller than 3% for all variations.

After calcination, PS cores were removed, resulting in hollow SiO_2 spheres. The hollow spheres were used for fabricating three-dimensional colloidal crystals (pathway I) via the capillary-deposition method,[24,25] revealing the high monodispersity and suspensibility of the hollow spheres. Alternatively, the core−shell

Received: October 14, 2011
Revised: December 16, 2011
Published: December 21, 2011

Scheme 1. Particle Formation and Colloidal Crystal Self-Assembly

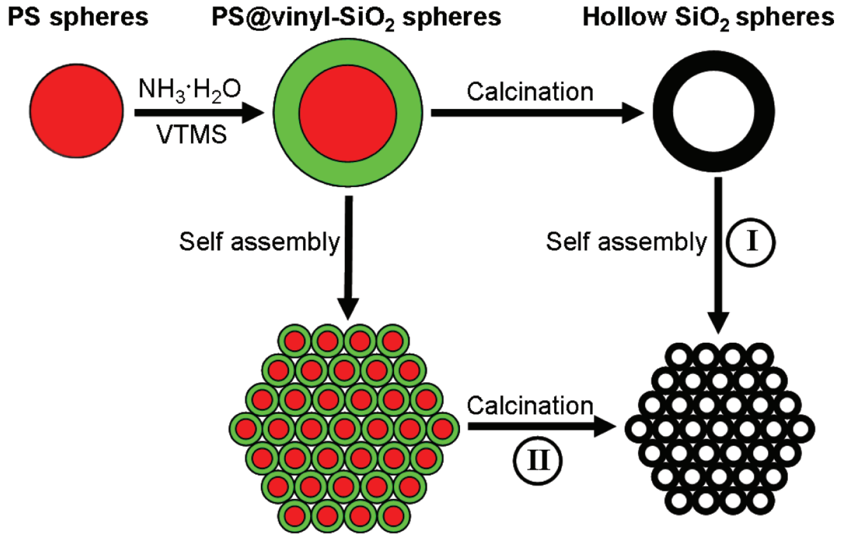

sphere colloidal crystals were converted into hollow sphere colloidal crystals by calcination (pathway II).

2. EXPERIMENTAL SECTION

2.1. Materials. The chemicals vinyltrimethoxysilane (VTMS, 98%, Sigma-Aldrich) and ammonia solution ($NH_3{\cdot}H_2O$, 28−30%, Merck, Germany) were used as received without further purification. PS particles (terminated with sulfate groups, negatively charged) with a specified diameter of (284 ± 10) nm (5 wt % aqueous suspension, named PS284) and (920 ± 23) nm (10 wt % aqueous suspension, named PS920) were purchased from Microparticles GmbH (Berlin). Ultrapure water (18.2 MΩ·cm) was directly used from a Milli-Q water system.

2.2. Synthesis. The vinyl-functionalized SiO_2 was coated on the surface of PS core following a modified Stöber process that involved the hydrolysis of VTMS in aqueous solution. For the preparation of core−shell particles, 0.35 mL of VTMS was added in 6.65 mL of H_2O under vigorous magnetic stirring for 30 min. The organic droplets were completely dissolved, and a transparent solution was obtained. Simultaneously, 15 mL of 0.5 wt % PS particles were mixed with 0.88 mL of ammonia under magnetic stirring for 5 min. Then, different amounts of the VTMS/H_2O mixture (see Table 1) were consecutively added into PS/NH_3/H_2O system. The reaction was allowed to proceed for 5 h at room temperature. The initial concentration of VTMS was as specified in Table 1, and the pH value was 11.5. After the completion of the reaction, the resulting particles were separated from the reaction medium by repeated centrifugation (3000 rpm) and ultrasonic dispersion (using ethanol) to remove ammonia, water, and unreacted VTMS.

Table 1. Core-Shell Spheres Obtained under Different Conditions[a]

sample	core particle	C_{VTMS} (mM)	$D_{v\text{-}Si}$ (nm)	$P_{v\text{-}Si}$ (%)	$t_{v\text{-}Si}$ (nm)
1	PS284	0	273	2.6	
2	PS284	50	289	2.5	11.1 ± 1.7
3	PS284	100	348	2.3	37.8 ± 3.5
4	PS284	150	406	2.4	64.9 ± 5.3
5	PS284	200	474	1.9	103.4 ± 4.3
6	PS284	250	622	1.4	174.6 ± 6.6
7	PS920	0	823	2.6	
8	PS920	120	907	1.3	45.1 ± 6.3

[a] $D_{v\text{-}Si}$, $P_{v\text{-}Si}$, and $t_{v\text{-}Si}$ mean diameter, polydispersity, and shell thickness of PS@vinyl-SiO_2 core-shell particles. The polydisperity P is defined by the relative standard deviation. $P = (\sum_{i=1}^{n}(D_i - D)^2/(n-1)/D\cdot 100\%)^{1/2}$, where D_i is the diameter obtained by measuring n particles using TEM.

The hollow SiO_2 spheres were obtained after removing the PS cores. The core−shell particles were heated to 550 °C at a rate of 2 °C/min, kept at 550 °C for 6 h in air, and then cooled to room temperature. The obtained hollow spheres were dispersed in ethanol for further usage.

2.3. Fabrication of Colloidal Crystals. The colloidal crystals were fabricated from redispersed particles (0.5 wt % in ethanol suspension) by using a capillary deposition method according to refs 24 and 25. The planar capillary cell contained two glass slides and was separated by two thin polymer spacers that could control the thickness of the film. One capillary tube was connected between the lower glass and the colloidal suspension and used to drag the suspension up into the planar cell, using the capillary force. The colloidal crystal film was formed in a few days along the open edges. The whole deposition process was carried out at nearly constant temperature ((22 ± 1) °C) and humidity ((40 ± 2) %).

2.4. Characterization. A transmission electron microscope (TEM) (Hitachi HF 2000) was used for observing the morphology and measuring the geometric parameters of the particles (about 50 particles for each sample). The samples were prepared by dipping a carbon coated copper grid into a diluted ethanol solution of particles, taking out the copper grid, and evaporating the ethanol solvent.

Dynamic light scattering (DLS) analysis was carried out on a Zetasizer Nano ZS system (Malvern).

The morphology of colloidal crystal films was observed using scanning electron microscopy (SEM) (Hitachi S-3500N). A thin Au layer (10 nm) was sputtered on the film before observing.

The solid-state ^{29}Si NMR spectra were recorded on a Bruker Avance 500WB spectrometer using a double-bearing standard MAS probe (DVT BL4) at resonance frequencies of 99.4 MHz.

Thermogravimetric analysis (TGA) was carried out on a TGA instrument (Netzsch STA 449C). The temperature was raised from room temperature to 1000 °C at a rate of 10 °C/min.

The transmission spectra of the colloidal crystals were performed using a Cary 5G UV−vis-NIR spectrometer (Varian).

3. RESULTS AND DISCUSSION

3.1. Overview. Figure 1a shows the TEM image of a typical sample of the core−shell particles prepared at VTMS concentration 100 mM (sample 3). The particle size is 348 nm with a very low polydispersity (P, see Table 1) of 2.3%. The inset in Figure 1a gives a high magnification TEM picture of core−shell structure showing that the vinyl-SiO_2 shells ((37.8 ± 3.5) nm) are uniformly coated on the surfaces of PS particles.

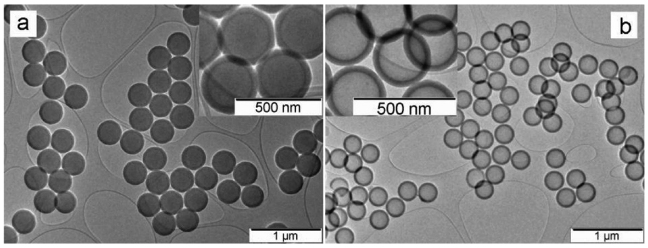

Figure 1. TEM images of the two particle types fabricated: (a) PS284@vinyl-SiO_2 core−shell particles (shell thickness 37.8 ± 3.5 nm) and (b) hollow SiO_2 spheres (shell thickness 33.5 ± 1.8 nm) obtained after calcination.

Figure 1b shows the hollow SiO_2 spheres obtained after calcining sample 3 at 550 °C for 6 h. The particle size is 296 nm with P = 1.9%. The inset in Figure 1b shows a clear hollow structure and uniform shell with the shell thickness of (33.5 ± 1.8) nm.

Generally, the size of core−shell particles could be adjusted by many parameters, such as the concentration of VTMS precursor/ammonia catalyst, the ratios of PS particles and VTMS precursor, the amount of water solvent, the reaction time, and the temperature. The reaction time and the concentration of precursor/catalyst have already been discussed in another work.[21] There, the concentration of precursor/catalyst was found to have significant influence on the particle size. Here, we focus on the influence of VTMS concentration (C_{VTMS}) on particle size and shell thickness. All the reactions were carried out at same pH at room temperature with constant stirring rate.

3.2. Core−Shell Particles. Figure 2 shows the TEM images of core−shell particles at different C_{VTMS}. By using C_{VTMS} from 50 mM to 250 mM, the shell thickness could be adjusted from ∼10 nm to ∼170 nm. The shell thickness (particle size) increased with increasing C_{VTMS}. The size, polydispersity, and shell thickness of the core−shell particles are listed in Table 1. It should be noted that C_{VTMS} seems to have a minimum value to form a uniform shell on the surface. We tried to use a C_{VTMS} of 25 mM, but no shell could be coated on the PS surface. It might be that the concentration of precursor is too low to form a shell, because of competing coating of macroscopic surfaces. C_{VTMS} = 50 mM is likely near to the lower limit to get a uniform shell on the PS surface.

We calculated the shell thickness theoretically. For that, we have assumed that the VTMS precursor reacted completely into vinyl-SiO_2. Furthermore, we have assumed that α_{con} (conversion ratio) of the vinyl-SiO_2 was coated onto the surface of the PS

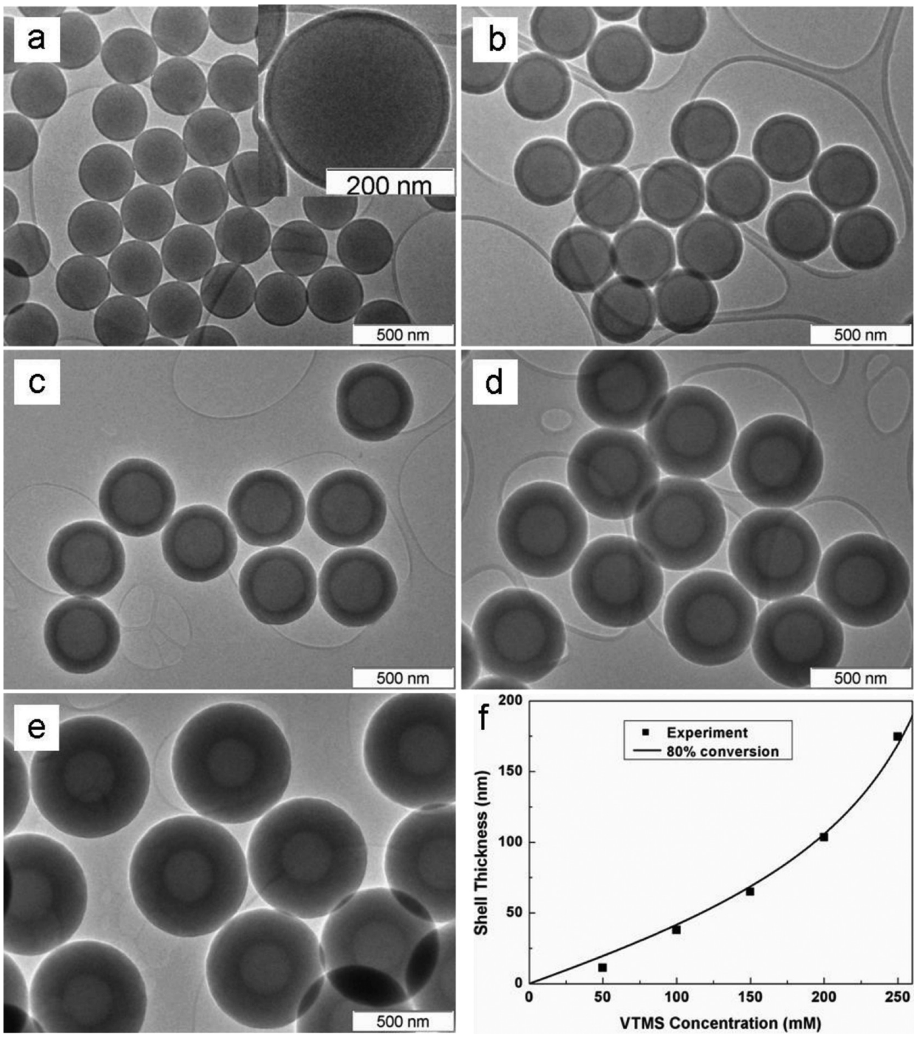

Figure 2. Control of the particle parameters. TEM images of PS284@vinyl-SiO_2 particles obtained from different C_{VTMS}: (a) 50 mM, (b) 100 mM, (c) 150 mM, (d) 200 mM, and (e) 250 mM. (f) The shell thickness $t_{\mathrm{v\text{-}Si}}$ as a function of C_{VTMS} measured by TEM (square dots) and expected curve for 80% conversion (black line) of the precursor (see text).

particles. We got the shell thickness $t_{\text{v-Si}}$ as a function of C_{VTMS}:

$$t_{\text{v-Si}} = \frac{d}{2}\left(\sqrt[3]{\frac{3.28\alpha_{\text{con}}C_{\text{VTMS}}}{314\ \text{mM} - C_{\text{VTMS}}} + 1} - 1\right) \qquad (1)$$

Here, d is the PS core diameter. The detailed derivation of eq 1 is given in the Supporting Information.

Figure 2f shows the shell thickness as a function of VTMS concentration. The experimental results are compared with eq 1 using $\alpha_{\text{con}} = 80\%$. The curve fits well the experimental data, which show a very steady behavior with concentration. Surprisingly, the fit was obtained for the conversion rate of 80%. The remaining 20% might easily be explained with coverage of the macroscopic surfaces (reaction vessel, stirring bar). This and the fact that no small particles have been found in the SEM pictures points to a coating process with a nearly perfect yield.

What could be the reason for this high coating yield? Normally, silica obtained in a Stöber-like process has a negative surface, which is not advantageous for coating on PS, which is also negatively charged (by sulfate groups coming from the polymerization initiator, product information for our particles). The use of organo-silica precursors will reduce the negative surface charge, but it cannot turn the charge situation significantly. Another influence of the precursor is on the hydrophobic/hydrophilic character of the generated surfaces. Normal Stöber-made silica is strongly hydrophilic because of OH groups at the surface. The organo-silica precursor leads to many fewer OH groups and also to hydrocarbon groups at the surface. Both reduce the hydrophilic character of the surface leading to higher interface tension. This enhances the critical seed size for particle formation. Because there are already surfaces offered by the PS in the system, the direct growth on them will become more likely in the organo-silica system. The proof of this mechanism needs, of course, more investigations (not in the scope of this paper), but the aspect connected with the number of OH groups can already be quantified by the NMR investigations (see the Supporting Information). Vinyl-SiO_2 has two silicon species (named T^2 and T^3) corresponding to $CH_2{=}CH{-}Si(OSi)_2(OH)$ and $CH_2{=}CH{-}Si(OSi)_3$ blocks.[26] Si is always connected with one vinyl group. The ratio of Si connected with OH groups in vinyl-SiO_2 particles is only 0.15 and, therefore, much less than that in Stöber-made pure SiO_2 where a ratio of 0.50 has been found.

3.3. Hollow Shell Formation.

The hollow SiO_2 spheres were obtained by calcining the core–shell particles in air at 550 °C for 6 h. The PS cores were burned away, and the remaining shell shrank a bit. As seen in Figure 3, highly monodisperse hollow spheres ($P < 3\%$) were obtained with shell thickness ranging from 30 to 150 nm. The particle size, polydispersity, and shell thickness of the hollow spheres are listed in Table 2.

In addition to the high monodispersity, the hollow SiO_2 spheres have another two promising characteristics. First, the shells have high mechanical stability, which can endure not only the calcination but also the ultrasonic and centrifugation treatments for several times. Second, the SiO_2 shells are suspensible in water or alcohol media, which could be used for further applications (see the next section).

DLS investigations were carried out for every resuspended sample. In each size distribution ranging from 0.1 to 10000 nm, only one peak appeared, indicating that there is no aggregation or destruction of particles in the dispersion within the sensitivity of the Zetasizer system. The DLS measurements are provided in the Supporting Information.

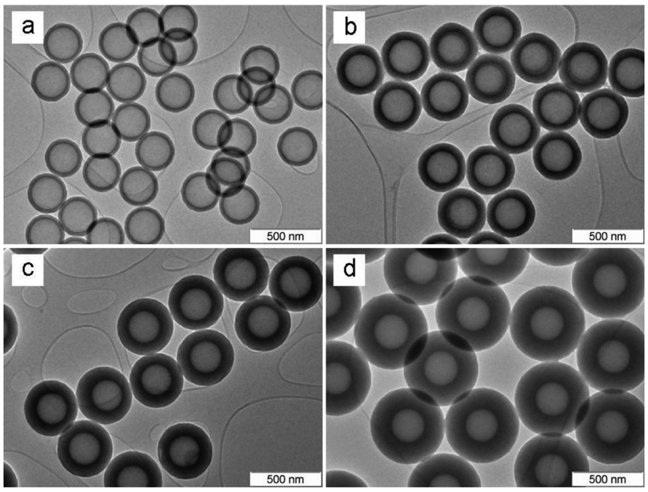

Figure 3. TEM images of hollow SiO_2 particles obtained from different C_{VTMS}: (a) 100 mM, (b) 150 mM, (c) 200 mM, and (d) 250 mM.

Table 2. Hollow SiO_2 Spheres Obtained after Calcination[a]

sample	core particle	C_{VTMS} (mM)	D_{Si} (nm)	P_{Si} (%)	t_{Si} (nm)
9	PS284	100	296	1.9	33.5 ± 1.8
10	PS284	150	339	2.4	60.1 ± 5.0
11	PS284	200	404	1.3	94.1 ± 3.6
12	PS284	250	531	1.0	151.8 ± 4.3
13	PS920	120	747	4.2	47.2 ± 6.7

[a] D_{Si}, P_{Si}, and t_{Si} mean diameter, polydispersity, and shell thickness of hollow SiO_2 particles measured by TEM.

As illustrated in Tables 1 and 2, both shell thickness and particle size of the hollow spheres are decreased, compared to parameters of the respective core–shell particles. Figure 4 plots the parameters of core–shell particles versus hollow spheres. The fact that the shell thickness and the particle size are reduced by the same factor shows a linear relationship. This means that the particles shrink isotropically during calcination.

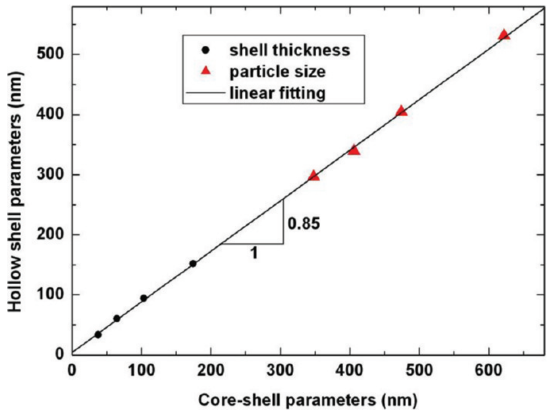

Figure 4. Comparison of core–shell particle parameters vs hollow sphere parameters of the shell thickness (●) and the particle size (▲).

For the sample obtained with $C_{\text{VTMS}} = 50$ mM, the shells could not fully be redispersed after calcination. The shells either remained aggregated, or they broke into parts. The calcination aggregates of the thin shells seem to be more stable during the ultrasound treatment and, if they are deaggregated, they cannot resist the stress in this process. This complicated behavior seems to generate a lower limit for the shell thickness.

The core−shell particle size was also changed by using different PS particles. Figure 5a shows a TEM image of core−shell particles made with PS920 as a core template. The particle size is 907 nm with $P = 1.3\%$. Figure 5b is the calcined sample with particle size 747 nm and $P = 4.2\%$. The increase of P can be ascribed to the deformation of the particles and some of hollow spheres, which are destroyed. The inset shows a destroyed shell. The mechanical stability of hollow spheres made from a bigger PS core template seems to be lower than that of smaller PS core templates.

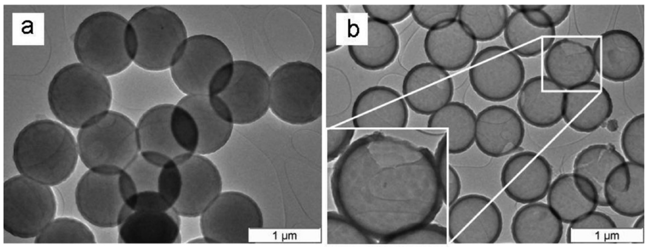

Figure 5. TEM images of (a) PS920@vinyl-SiO_2 core−shell particles with a shell thickness of (45.1 ± 6.3) nm obtained at $C_{VTMS} = 120$ mM, and (b) hollow SiO_2 spheres with a shell thickness of (47.2 ± 6.7) nm obtained after calcination. Inset: an exceptional broken particle that shows the hollow structure clearly.

To study the calcination process of the hybrid core−shell particles, TGA was performed under air atmosphere with a rate of 10 °C/min. Figure 6 shows the TG curves of three samples: PS284, vinyl-SiO_2, and PS@vinyl-SiO_2. The pure PS particles are fully decomposed after calcination. Vinyl-SiO_2 shows an initial weight increase and then a loss. The partial oxidation of vinyl groups beginning at ∼200 °C causes the weight increase, and the later weight loss can be attributed to the degradation of organic parts. The final residue is 74.1%. This residue can also be estimated theoretically. We assume that both of the species T^2 ($CH_2{=}CH{-}Si(OSi)_2(OH)$) and T^3 ($CH_2{=}CH{-}Si(OSi)_3$), are totally converted into pure silica after calcination. The exact chemical composition of vinyl-SiO_2 can be deduced from T^2 and T^3 in the NMR spectrum. The residue calculated in this way (74.8%) is in accordance with the experimental result. This means the vinyl groups are totally burned away.

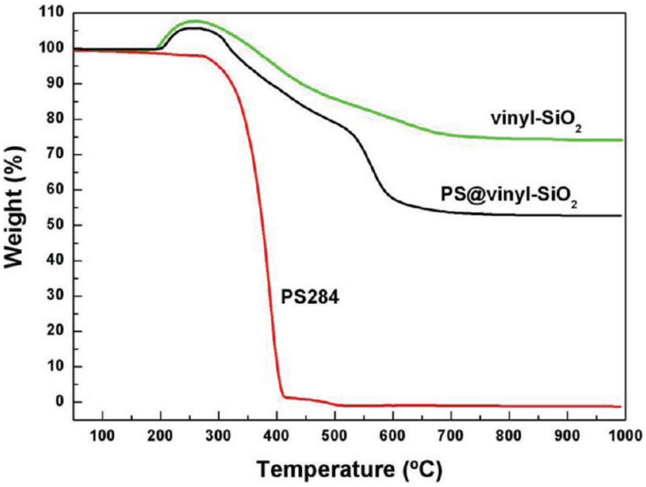

Figure 6. TG curves of PS284 particles, vinyl-SiO_2 particles, and PS@vinyl-SiO_2 particles (PS284, $t_{v\text{-}Si} = 52.1$ nm).

The TG curve of the PS@vinyl-SiO_2 possesses partial characteristics of PS and vinyl-SiO_2. First, it also has a weight increase stage beginning at ∼200 °C, but the increment is lower than that of the vinyl-SiO_2 because only the shell part can cause the weight increase. Second, it has a delayed decomposition of PS material (∼500 °C − 600 °C), compared to the PS particles (fully decomposed at ∼500 °C). The reason for this is likely that the PS core is protected by the vinyl-SiO_2 shell, which slows down the PS decomposition speed. With the increase of the temperature, a porous structure might be formed after the removal of the vinyl group from the vinyl-SiO_2, which could let the decomposed PS pass through the SiO_2 shell. Third, it has lower residue compared to the vinyl-SiO_2 due to the removal of PS cores after calcination. The value is in accordance with theory.

3.4. Colloidal Crystal Assembly and Characterization.

The traditional way to realize the colloidal crystals of hollow shells (hs-CCs) involves two processes: the formation of colloidal crystals of core−shell particles and the removal of the cores.[27−32] Calcination[27,28] and chemical etching[29−32] are the two methods to remove the cores. However, an increased number of defects such as cracks and distorted regions are generated after this step. Therefore, direct formation of hs-CCs by hollow spheres might be a way to get better crystals. Hollow PS spheres have already been used for assembling high-quality hs-CCs.[33,34] However, the hollow PS spheres have the limitation of low mechanical and thermal stability. Here, we used hollow SiO_2 spheres for fabricating colloidal crystals.

Three kinds of colloidal crystals were prepared for comparison: colloidal crystals (1) assembled from PS@vinyl-SiO_2 core−shell particles (c-s-CCs), (2) assembled from hollow SiO_2 spheres (pathway I, named hs-CCs-I), and (3) obtained by calcining the c-s-CCs (pathway II, named hs-CCs-II).

Figure 7a−c shows typical SEM images of the three samples with the same magnification. The hs-CCs-I has a better structure than the hs-CCs-II, which is visible in smaller and fewer cracks. The increase in the number of cracks in hs-CCs-II can be ascribed to the shrinkage of the particles during the calcination process.

Figure 7d shows the transmission spectra of the colloidal crystals. The c-s-CCs have a strong intensity of the stop band, while the intensity of both the hs-CCs-I and hs-CCs-II is very weak. We assign this to the smaller effective modulation of the refractive index because the high-index material is only a thin layer. Compared to the c-s-CCs, the stop band of the hs-CCs-II had an obvious blue-shift. This is due to the decease of the effective refractive index (n_{eff}) and particle size during calcination. Simultaneously, the bandwidth and background are increased, likely because the amount of defects is increased.

Interestingly, hs-CCs-I have exactly the same stop band as the hs-CCs-II. This means that the two ways of preparing hs-CCs result in the same lattice constant and n_{eff}. In other words, there were same changes in n_{eff} and particle size during the calcination of core−shell particles and the c-s-CCs. However, the bandwidth and background of hs-CCs-I were much less than that of the hs-CCs-II. We connect this with the amount of defects.

Another interesting point is that Fabry−Pérot fringes were observed in the transmission spectrum of hs-CCs-I, as shown in the inset of Figure 7d. To our knowledge, there is no report on

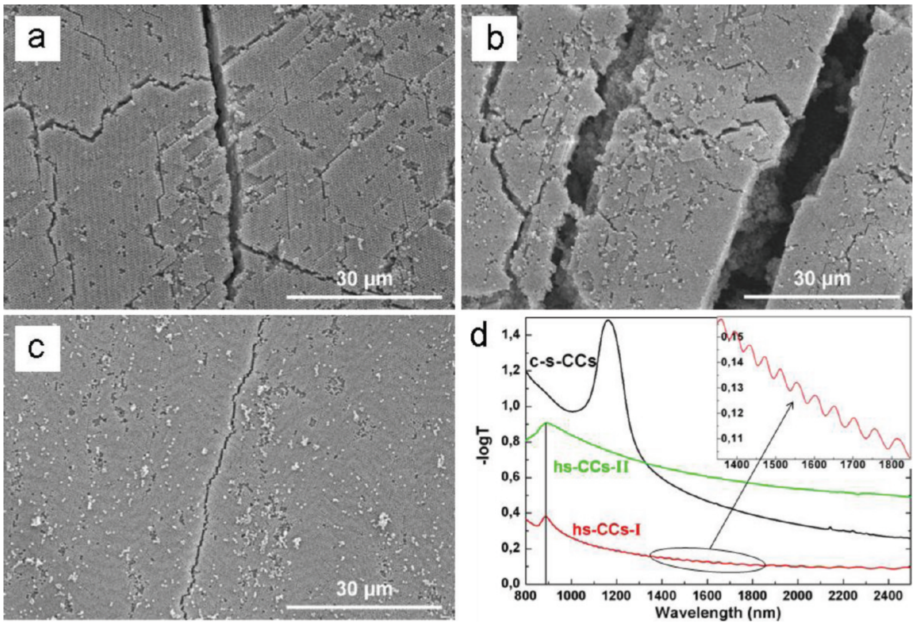

Figure 7. SEM images of (a) colloidal crystals self-assembled from PS@vinyl-SiO_2 core−shell spheres (c-s-CCs), (b) calcined core−shell colloidal crystals (hs-CCs-II), and (c) colloidal crystals directly assembled from hollow SiO_2 spheres (hs-CCs-I). (d) Transmission spectra of (a), (b), and (c). Inset in part d: magnified spectrum of hs-CCs-I.

this for thick colloidal crystals. Our crystals have a thickness of 23 μm, which is equal to about 70 layers. Thus, the hs-CCs obtained from direct assembly of hollow spheres have exceptionally high quality. This enhanced quality might be ascribed to the high mechanical flexibility of the hollow spheres, but it is possibly also ascribable to reduced disturbing sedimentation effects during deposition.

4. CONCLUSIONS

We have demonstrated a method for coating a uniform vinyl-SiO_2 shell on negatively charged PS particles. Highly monodisperse ($P < 3\%$) core−shell particles with shell thicknesses ranging from 10 to 170 nm were obtained.

After calcination, monodisperse hollow SiO_2 spheres with shell thicknesses from 30 to 150 nm were obtained. Beside the mechanical stability and the high monodispersity, the hollow SiO_2 spheres are also suspensible in water and alcohol media. Thus, the hollow SiO_2 spheres can efficiently be used for making colloidal crystals. The colloidal crystals obtained in this way have the same reduced background scattering and better shaped Bragg peaks as those obtained by alternative pathways. This and the observed Fabry−Pérot oscillations in transmission spectra indicate an exceptionally high crystalline quality.

The synthesis method might be extended for coating uniform organo-SiO_2 shells on different kinds of core materials. In addition, the use of other organo-oxide precursors could lead to new hollow oxide particles useful for colloidal crystal formation.

■ ASSOCIATED CONTENT

Ⓢ Supporting Information

^{29}Si NMR spectra of SiO_2 particles and vinyl-SiO_2 particles, size distributions of core−shell particles and hollow SiO_2 spheres by DLS measurements, and the derivation of the shell thickness as function of VTMS concentration. This material is available free of charge via the Internet at http://pubs.acs.org.

■ AUTHOR INFORMATION

Corresponding Author

*Telephone: 49-208-3062255. Fax: 49-208-3062995. E-mail: marlow@mpi-muelheim.mpg.de.

■ ACKNOWLEDGMENTS

The authors thank Dr. Wolfgang Schmidt for TG measurements, Dr. Bodo Zibrowius for NMR measurements and discussions, Rainer Brinkmann for providing Stöber particles, Bernd Spliethoff, Hans-Josef Bongard, and Silvia Palm for their extensive electron microscopy support and discussions.

■ REFERENCES

(1) Guerrero-Martínez, A.; Pérez-Juste, J.; Liz-Marzán, L. M. *Adv. Mater.* **2010**, *22*, 1182−1195.

(2) Zou, H.; Wu, S.; Shen, J. *Chem. Rev.* **2008**, *108*, 3893−3957.

(3) Hoffmann, F.; Cornelius, M.; Morell, J.; Fröba, M. *Angew. Chem., Int. Ed.* **2006**, *45*, 3216−3251.

(4) Slowing, I. I.; Trewyn, B. G.; Giri, S.; Lin, V. S.-Y. *Adv. Funct. Mater.* **2007**, *17*, 1225−1236.

(5) Marlow, F.; Muldarisnur.; Sharifi, P.; Brinkmann, R.; Mendive, C. *Angew. Chem., Int. Ed.* **2009**, *48*, 6212−6233.

(6) Wong, Y. J.; Zhu, L.; Teo, W. S.; Tan, Y. W.; Yang, Y.; Wang, C.; Chen, H. *J. Am. Chem. Soc.* **2011**, *133*, 11422−11425.

(7) Han, Y.; Jiang, J.; Lee, S. S.; Ying, J. Y. *Langmuir* **2008**, *24*, 5842−5848.

(8) Mahtab, F.; Yu, Y.; Lam, J. W. Y.; Liu, J.; Zhang, B.; Lu, P.; Zhang, X.; Tang, B. Z. *Adv. Funct. Mater.* **2011**, *21*, 1733−1740.

(9) Jing, L.; Yang, C.; Qiao, R.; Niu, M.; Du, M.; Wang, D.; Gao, M. *Chem. Mater.* **2010**, *22*, 420−427.

(10) Lu, Y.; McLellan, J.; Xia, Y. *Langmuir* **2004**, *20*, 3464−3470.

(11) Qi, G.; Wang, Y.; Estevez, L.; Switzer, A. K.; Duan, X.; Yang, X.; Giannelis, E. P. *Chem. Mater.* **2010**, *22*, 2693−2695.

(12) Hong, J.; Lee, J.; Rhymb, Y. M.; Kim, D. H.; Shim, S. E. *J. Colloid Interface Sci.* **2010**, *344*, 410−416.

(13) Graf, C.; Vossen, D. L. J.; Imhof, A.; Blaaderen, A. v. *Langmuir* **2003**, *19*, 6693−6700.

(14) Caruso, F.; Caruso, R. A.; Möhwald, H. *Science* **1998**, *282*, 1111−1114.

(15) Sun, B.; Mutch, S. A.; Lorenz, R. M.; Chiu, D. T. *Langmuir* **2005**, *21*, 10763−10769.

(16) Tissot, I.; Reymond, J. P.; Lefebvre, F.; Bourgeat-Lami, E. *Chem. Mater.* **2002**, *14*, 1325−1331.

(17) Shin, K.; Kim, J. J.; Suh, K. D. *J. Colloid Interface Sci.* **2010**, *350*, 581−585.

(18) Tan, B.; Rankin, S. E. *Langmuir* **2005**, *21*, 8180−8187.

(19) Leng, W.; Chen, M.; Zhou, S.; Wu, L. *Langmuir* **2010**, *26*, 14271−14275.

(20) Stöber, W.; Fink, A.; Bohn, E. *J. Colloid Interface Sci.* **1968**, *26*, 62−69.

(21) Deng, T. S.; Zhang, Q. F.; Zhang, J. Y.; Shen, X.; Zhu, K. T.; Wu, J. L. *J. Colloid Interface Sci.* **2009**, *329*, 292−299.

(22) Deng, T. S.; Zhang, J. Y.; Zhu, K. T.; Zhang, Q. F.; Wu, J. L. *Colloids Surf. A* **2010**, *356*, 104−111.

(23) Deng, T. S.; Zhang, J. Y.; Zhu, K. T.; Zhang, Q. F.; Wu, J. L. *Mater. Chem. Phys.* **2011**, *129*, 540−546.

(24) Li, H.-L.; Dong, W.; Bongard, H.-J.; Marlow, F. *J. Phys. Chem. B* **2005**, *109*, 9939−9945.

(25) Muldarisnur, M.; Marlow, F. *J. Phys. Chem. C* **2011**, *115*, 414−418.

(26) Sindorf, D. W.; Maciel, G. E. *J. Am. Chem. Soc.* **1983**, *105*, 3767−3776.

(27) Wang, L.; Asher, S. A. *Chem. Mater.* **2009**, *21*, 4608−4613.

(28) Hosein, I. D.; Liddell, C. M. *Langmuir* **2007**, *23*, 2892−2897.

(29) Míguez, H.; Tetreault, N.; Yang, S. M.; Kitaev, V.; Ozin, G. A. *Adv. Mater.* **2003**, *15*, 597−600.

(30) García-Santamaría, F.; Ibisate, M.; Rodriguez, I.; Meseguer, F.; López, C. *Adv. Mater.* **2003**, *15*, 788−792.

(31) Blanco, A.; López, C. *Adv. Mater.* **2006**, 1593−1597.

(32) Rengarajan, R.; Jiang, P.; Colvin, V.; Mittleman, D. *Appl. Phys. Lett.* **2000**, *77*, 3517−3519.

(33) Xu, X.; Asher, S. A. *J. Am. Chem. Soc.* **2004**, *126*, 7940−7945.

(34) Nakamura, H.; Ishii, M. *J. Appl. Polym. Sci.* **2007**, *103*, 2364−2368.

Supporting Information.

Synthesis of Monodisperse Polystyrene@Vinyl-SiO_2 Core-Shell Particles and Hollow SiO_2 Spheres

Tian-Song Deng, Frank Marlow*

*Corresponding author. E-mail: marlow@mpi-muelheim.mpg.de.

1. NMR investigations

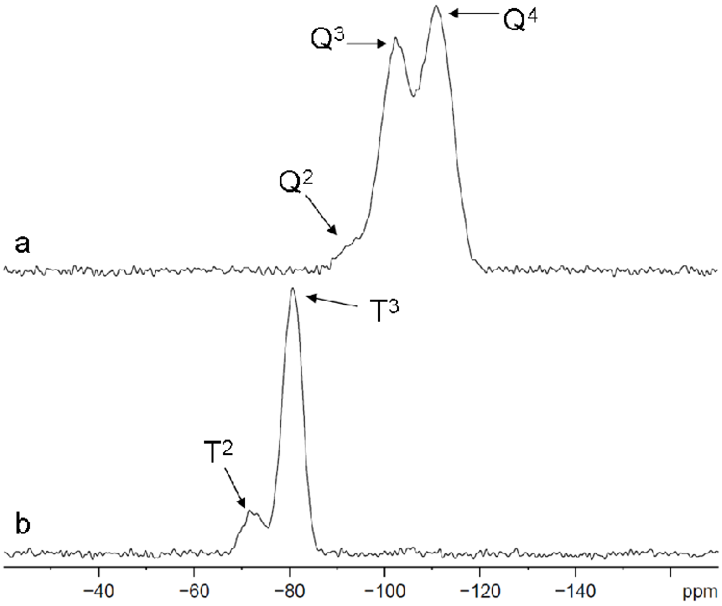

Figure S1. ^{29}Si CP-MAS NMR spectrum of (a) SiO_2 particles (Stöber method[20], dried) and (b) vinyl-SiO_2 particles.

The connection of silicon atoms and vinyl groups (CH_2=CH-Si) in vinyl-SiO_2 can be confirmed by comparison of solid-state ^{29}Si CP-MAS NMR spectra of SiO_2 and vinyl-SiO_2 (Figure S1). The SiO_2 spectrum in Figure S1a has three Q-species corresponding to Q^2 (-93.4 ppm), Q^3 (-102.2 ppm) and Q^4 (-111.0 ppm), representing ($Si(OSi)_2(OH)_2$), ($Si(OSi)_3(OH)$), and ($Si(OSi)_4$), respectively. The vinyl-SiO_2 spectrum (Figure S1b) only has two T-species corresponding to T^2 (-71.5 ppm) and T^3 (-80.5 ppm), where T^2 represents CH_2=CH-$Si(OSi)_2(OH)$ species and T^3 represents CH_2=CH-$Si(OSi)_3$ species.[26] This indicates that Si is always connected with vinyl groups. The amount of vinyl groups is the same as silicon atoms. Furthermore, the ratio of OH groups ($T^2/(T^2+T^3)=0.15$) in vinyl-SiO_2 particles is much less than that in SiO_2 particles ($(2Q^2+Q^3)/(2Q^2+Q^3+Q^4)=0.50$).

2. DLS investigations

Figures S2-S14 are the size distributions of the particles from PS@vinyl-SiO_2 core-shell particles and hollow SiO_2 spheres (samples 1-13). Only one peak appeared in every DLS spectrum from 0.1 nm to 10000 nm. There was no sign for aggregates or broken parts of the particles. Because of the apparatus effect, the polydispersities resulted from DLS measurements are much larger than those from SEM. Therefore, we did not give the polydispersities here.

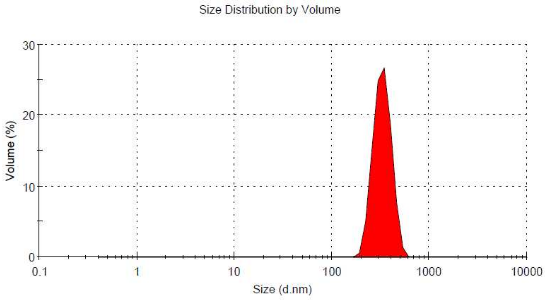

Figure S2. PS284 in water, 0 mM VTMS, D^{DLS}=318 nm.

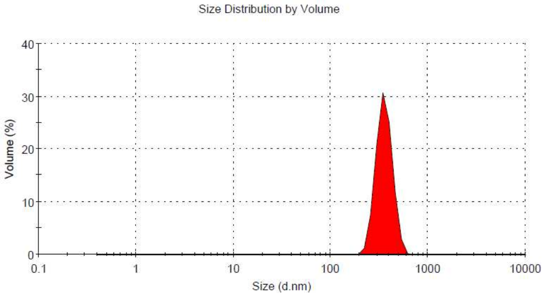

Figure S3. Core-shell particles in ethanol, core: PS284, 50 mM VTMS, D^{DLS}=348 nm.

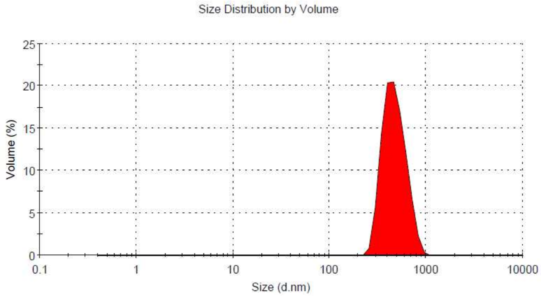

Figure S4. Core-shell particles in ethanol, core: PS284, 100mM VTMS, D^{DLS}=467 nm.

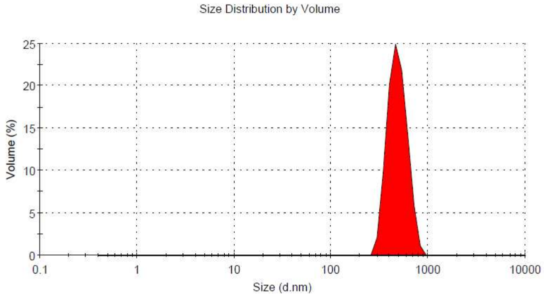

Figure S5. Core-shell particles in ethanol, core: PS284, 150mM VTMS, D^{DLS}=487 nm.

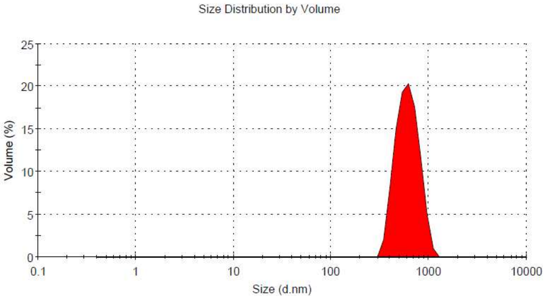

Figure S6. Core-shell particles in ethanol, core: PS284, 200mM VTMS, D^{DLS}=580 nm.

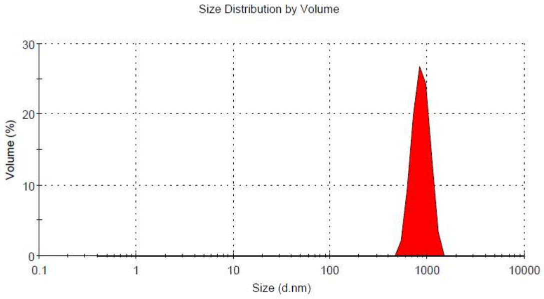

Figure S7. Core-shell particles in ethanol, core: PS284, 250mM VTMS, D^{DLS}=810 nm.

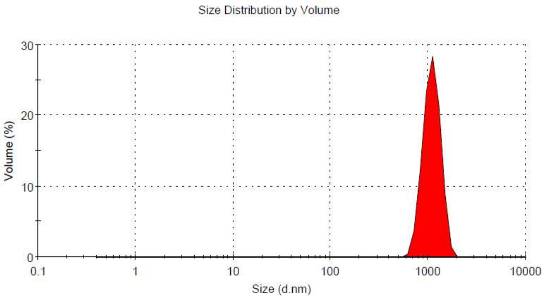

Figure S8. PS920 in water, 0 mM VTMS, D^{DLS}=1002 nm.

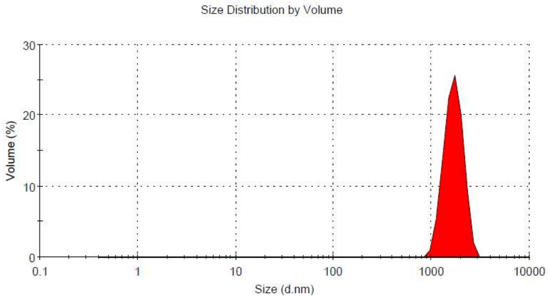

Figure S9. Core-shell particles in ethanol, core: PS920, 120mM VTMS, D^{DLS}=1532 nm.

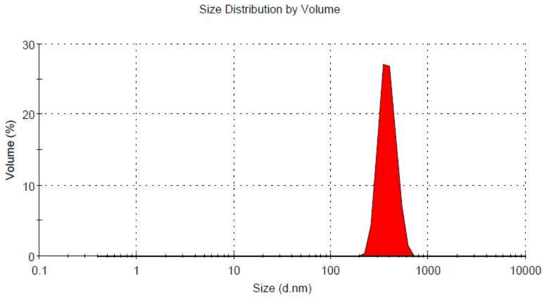

Figure S10. Hollow SiO2 spheres in ethanol, core: PS284, 100mM VTMS, D^{DLS}=377 nm.

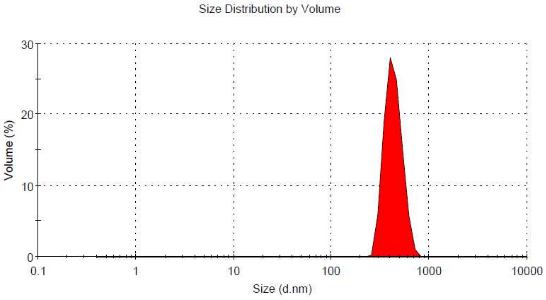

Figure S11. Hollow SiO2 spheres in ethanol, core: PS284, 150mM VTMS, D^{DLS}=429 nm.

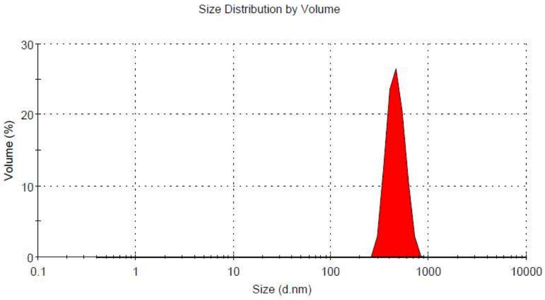

Figure S12. Hollow SiO2 spheres in ethanol, core: PS284, 200mM VTMS, D^{DLS}=465 nm.

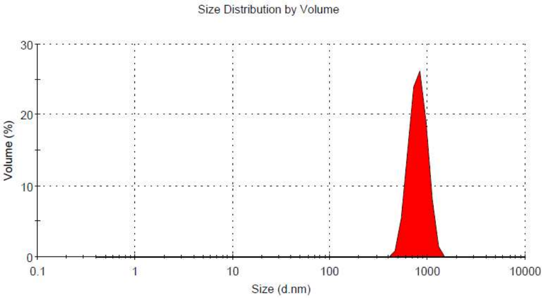

Figure S13. Hollow SiO2 spheres in ethanol, core: PS284, 250mM VTMS, D^{DLS}=739 nm.

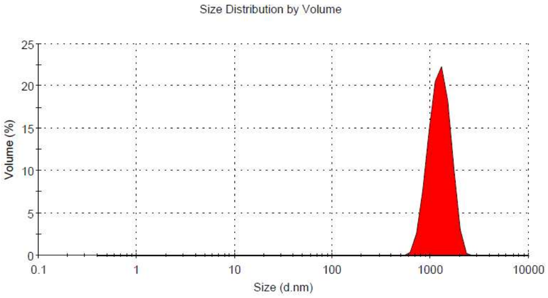

Figure S14. Hollow SiO2 spheres in ethanol, core: PS920, 120 mM VTMS, D^{DLS}=1055 nm.

3. The shell thickness as a function of VTMS precursor concentration

(1) Relationship between concentration C_{VTMS} and volume of VTMS V_{VTMS}

A volume of V_{VTMS} VTMS was added to $19V_{VTMS}$ H_2O under vigorous magnetic stirring for 30 min. The organic droplets were completely dissolved and a transparent VTMS/H_2O solution ($20V_{VTMS}$) was obtained. Simultaneously, a volume V_{PS} of 0.5% PS284 particles was mixed with an ammonia solution volume of $V_{ammonia} = (20V_{VTMS}+V_{PS})/25$ to keep the pH=11.5 for every experiment. Then

$$V = 20V_{VTMS} + V_{PS} + V_{ammonia} = \frac{26}{25}(20V_{VTMS} + V_{PS}) \tag{1}$$

V is the total volume of reaction system. According to equation 1, we get

$$C_{VTMS} = \frac{m_{VTMS}}{M_{VTMS} \cdot V} = \frac{\rho_{VTMS} \cdot V_{VTMS}}{M_{VTMS} \cdot \frac{26}{25}(20V_{VTMS} + V_{PS})} \tag{2}$$

Here m_{VTMS} and ρ_{VTMS} are the mass and density of VTMS, and M_{VTMS} is the molecular weight of VTMS. Then

$$V_{VTMS} = \frac{26 \cdot M_{VTMS} \cdot V_{PS} \cdot C_{VTMS}}{25\rho_{VTMS} - 520 \cdot M_{VTMS} \cdot C_{VTMS}} \tag{3}$$

(2) The mass of vinyl-SiO_2 $m_{v\text{-}Si}$

If 1 mol VTMS reacts completely, 1 mol vinyl-SiO_2 is obtained.
Therefore,

$$\frac{m_{v-Si}}{M_{v-Si}} = \frac{m_{VTMS}}{M_{VTMS}} = \frac{\rho_{VTMS} \cdot V_{VTMS} \cdot w}{M_{VTMS}} \tag{4}$$

Here $M_{v\text{-}Si}$ is the molecular weight of vinyl-SiO_2, and w is the mass fraction of pure VTMS in the used commercial VTMS chemical. Then we find,

$$m_{v-Si} = \frac{M_{v-Si} \cdot \rho_{VTMS} \cdot w}{M_{VTMS}} \cdot V_{VTMS} \tag{5}$$

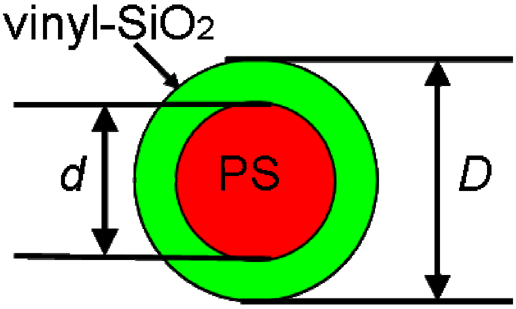

Figure S14. Scheme of PS@vinyl-SiO_2 particles.

(3) Particle size D and $m_{v\text{-}Si}$

N PS spheres with a diameter d and a density ρ_{PS} have a total mass m_{PS} of:

$$m_{PS} = N \cdot \rho_{PS} \cdot \frac{1}{6}\pi d^3 \tag{6}$$

We assume that α_{con} (conversion ratio) of the vinyl-SiO_2 could be homogeneously coated on the surface of PS core. Then

$$m_{v-Si} \cdot \alpha_{con} = N \cdot \rho_{v-Si} \cdot [\frac{1}{6}\pi D^3 - \frac{1}{6}\pi d^3] \tag{7}$$

According to equations 6 and 7, we get

$$\frac{m_{v-Si} \cdot \alpha_{con}}{m_{PS}} = \frac{N \cdot \rho_{v-Si} \cdot (D^3 - d^3)}{N \cdot \rho_{PS} \cdot d^3} = \frac{\rho_{v-Si}}{\rho_{PS}} \cdot (\frac{D^3}{d^3} - 1) \tag{8}$$

$$\Rightarrow D = d \cdot \sqrt[3]{\frac{\rho_{PS} \cdot \alpha_{con}}{m_{PS} \cdot \rho_{v-Si}} \cdot m_{v-Si} + 1} \tag{9}$$

(4) Shell thickness $t_{v\text{-}Si}$

According to the equations 3, 5, and 9, we can get

$$D = d \cdot \sqrt[3]{\frac{26 \cdot w \cdot \rho_{PS} \cdot \rho_{VTMS} \cdot M_{v-Si} \cdot V_{PS} \cdot \alpha_{con} \cdot C_{VTMS}}{m_{PS} \cdot \rho_{v-Si} \cdot (25 \cdot \rho_{VTMS} - 520 \cdot M_{VTMS} \cdot C_{VTMS})} + 1} \tag{10}$$

Specifying equation 10 with the data $w = 0.98$, $\rho_{PS} = 1.05$ g/cm^3, $\rho_{VTMS} = 0.968$ g/mL, $M_{v\text{-}Si} = 79.14$ g/mol, $V_{PS} = 15$ mL, $m_{PS} = 0.075$ g, $\rho_{v\text{-}Si} = 1.62$ g/cm^3, and $M_{VTMS} = 148.23$ g/mol resulted in

$$D = d \cdot \sqrt[3]{\frac{3.28 \cdot \alpha_{con} \cdot C_{VTMS}}{314 \text{ mM} - C_{VTMS}} + 1} \tag{11}$$

Because of $D = d + 2t_{v\text{-}Si}$, we get for the shell thickness:

$$t_{v-Si} = \frac{d}{2} \cdot (\sqrt[3]{\frac{3.28 \cdot \alpha_{con} \cdot C_{VTMS}}{314 \text{ mM} - C_{VTMS}} + 1} - 1) \tag{12}$$